Discontinuity analysis of the leading switchback transition regions

M. Akhavan-Tafti, J. Kasper, J. Huang, S. Bale

A&A 650, A4 (2021)
https://doi.org/10.1051/0004-6361/202039508

Astronomy & Astrophysics

Parker Solar Probe: Ushering a new frontier in space exploration

Special issue

Discontinuity analysis of the leading switchback transition regions

M. Akhavan-Tafti[1,2], J. Kasper[1], J. Huang[1], and S. Bale[3]

[1] Climate and Space Sciences and Engineering (CLaSP), University of Michigan, Ann Arbor, MI, USA
e-mail: akhavant@umich.edu
[2] Laboratoire de Physique des Plasmas (LPP), École Polytechnique, Centre national de la recherche scientifique (CNRS), Sorbonne Université, Institut Polytechnique de Paris, Palaiseau, France
[3] University of California, Space Science Laboratory, Berkeley, CA, USA

Received 23 September 2020 / Accepted 16 February 2021

ABSTRACT

Context. Magnetic switchbacks are magnetic structures characterized as intervals of sudden reversal in the radial component of the pristine solar wind's magnetic field. Switchbacks comprise of magnetic spikes that are preceded and succeeded by switchback transition regions within which the radial magnetic field reverses. Determining switchback generation and evolution mechanisms will further our understanding of the global circulation and transportation of the Sun's open magnetic flux.
Aims. The present study juxtaposes near-Sun switchback transition regions' characteristics with similar magnetic discontinuities observed at greater radial distances with the goal of determining local mechanism(s) through which switchback transition regions may evolve.
Methods. Measurements from fields and plasma suites aboard the Parker Solar Probe were utilized to characterize switchback transition regions. Minimum variance analysis (MVA) was applied on the magnetic signatures of the leading switchback transition regions. The leading switchback transition regions with robust MVA solutions were identified and categorized based on their magnetic discontinuity characteristics.
Results. It is found that 78% of the leading switchback transition regions are rotational discontinuities (RD). Another 21% of the leading switchback transition regions are categorized as "either" discontinuity (ED), defined as small relative changes in both magnitude and the normal component of the magnetic field. The RD-to-ED event count ratio is found to reduce with increasing distance from the Sun. The proton radial temperature sharply increases (+29.31%) at the leading RD-type switchback transition regions, resulting in an enhanced thermal pressure gradient. Magnetic curvature at the leading RD-type switchback transition regions is often negligible. Magnetic curvature and the thermal pressure gradient are parallel (i.e., "bad" curvature) in 74% of the leading RD-type switchback transition regions.
Conclusions. The leading switchback transition regions may evolve from RD-type into ED-type magnetic discontinuities while propagating away from the Sun. Local magnetic reconnection is likely not the main driver of this evolution. Other drivers, such as plasma instabilities, need to be investigated to explain the observed significant jump in proton temperature and the prevalence of bad curvature at the leading RD-type switchback transition regions.

Key words. magnetic reconnection – magnetic fields – solar wind – methods: data analysis – magnetohydrodynamics (MHD) – instabilities

1. Introduction

Magnetic switchbacks (Kahler et al. 1996; McComas et al. 1996; Yamauchi et al. 2004; Suess 2007; Matteini et al. 2014; Borovsky 2016) were identified in Ulysses' observations of high-latitude solar coronal holes. They describe intervals of intermittent reversals in the radial component of the magnetic field. The Parker Solar Probe (PSP; Fox et al. 2016) observations in the near-ecliptic plane have provided further evidence for magnetic switchbacks associated with Alfvénic jets of plasma (Bale et al. 2019; Kasper et al. 2019) and enhanced Poynting flux (Mozer et al. 2020) in the near-Sun environment. Switchbacks last seconds to hours in duration. Various studies have explored the possible origin(s) of switchbacks (Squire et al. 2020; Drake et al. 2021; Horbury et al. 2020).

There are four types of magnetic discontinuities in the solar wind. The two most commonly observed types are rotational discontinuities (RDs) and tangential discontinuities (TDs). At 1 AU, solar wind magnetic discontinuities are observed on average once every hour. Their average duration is ~2 s (Tsurutani & Smith 1979).

Tangential discontinuities are non-propagating structures and are purely convected by solar wind (Tsurutani et al. 2011). They are characterized by net-zero normal mass flux ($[\rho V_{\rm Norm}] = 0$) and total pressure ($[P_{\rm Total}] = [P_{\rm th} + P_{\rm B}] = 0$) across the discontinuity, where $[x]$ denotes the change in x across the discontinuity. Furthermore, $P_{\rm th}$ and $P_{\rm B}$ represent thermal and magnetic pressures, respectively. In contrast, RDs are characterized as having $[\rho V_{\rm Norm}] \neq 0$, $[B_{\rm Norm}] \neq 0$, and $[B_{\rm Tangential}] = 0$.

Rotational discontinuities and TDs differ in one essential respect: magnetic connectivity across the discontinuity. In an RD, the two sides of the discontinuity are magnetically connected, as one component of the upstream magnetic field is parallel to the normal of the discontinuity plane. In contrast,

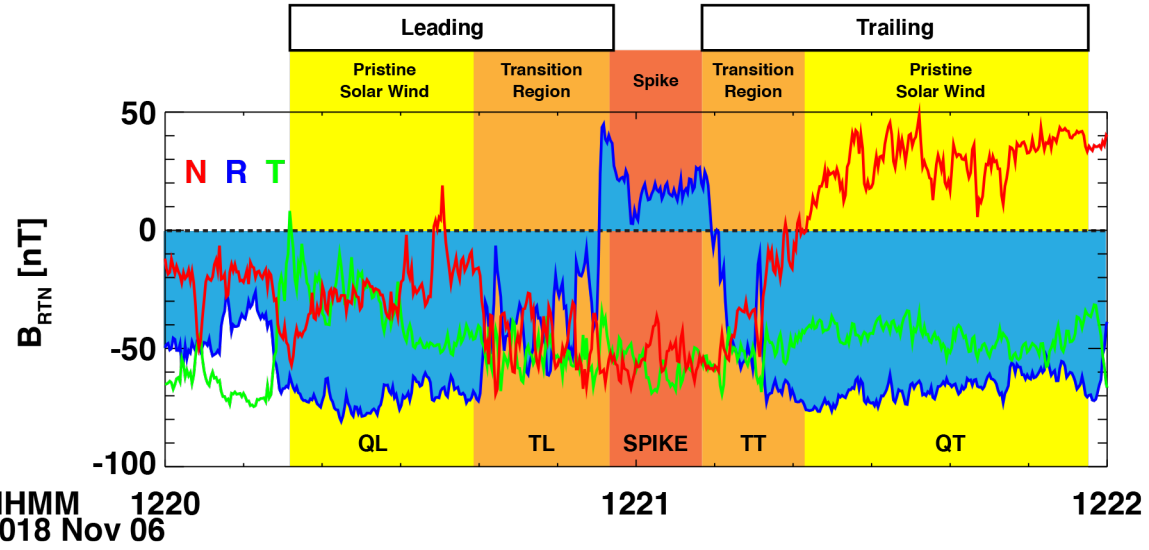

Fig. 1. Magnetic field profile of a magnetic switchback event in RTN coordinates during the first PSP encounter. A switchback comprises a magnetic spike that is separated from the pristine solar wind by a transition region. The radial component of the magnetic field reverses inside the transition region. The interval is 120 s in duration.

magnetic fields on either side of a TD lie on parallel planes. In other words, TD separates two distinct plasma regimes, allowing no plasma to flow across the discontinuity (Tsurutani et al. 2011). On the other hand, plasma transport is permitted across an RD.

Yamauchi et al. (2002) analyzed pressure balance structures (PBSs) with and without radially "folded back" magnetic fields wherein changes in the plasma and magnetic pressures balance one another out and the total pressure remains constant (McComas et al. 1996). The authors identified PBSs in the high-speed solar wind from polar coronal hole using Ulysses measurements at 2.9 AU. The minimum variance analysis technique (MVA; Sonnerup & Cahill Jr 1967) was applied to the region between the quiet solar wind and magnetic spike, where the radial magnetic field changes sign, hereon referred to as the magnetic transition region (Kasper et al. 2019).

Using numerical magnetohydrodynamic simulations, Tenerani et al. (2020) show that magnetic switchbacks become increasingly unstable and eventually decay as they propagate away from the Sun. Switchbacks evolve to release their magnetic tension and reach pressure equilibrium with their surrounding environment (Landi et al. 2005). The open science question is whether switchbacks evolve via adiabatic relaxation or nonadiabatic mechanisms, such as magnetic reconnection. The answer to this question will further our understanding of plasma acceleration and heating mechanisms in the solar wind.

In this study, we analyze all switchbacks in the first PSP encounter. MVA was applied on switchback transition regions to understand their spatial orientations. Discontinuity analyses were further performed on switchback transition regions to shed light on the evolution of switchbacks as they propagate away from the Sun.

2. Results

The present study utilizes magnetic field (FIELDS; Bale et al. 2016) and plasma (SWEAP; Kasper et al. 2016) instruments aboard PSP. During the first encounter, PSP was on a solar orbit with its first perihelion at 36 solar radii.

Figure 1 shows a magnetic switchback comprising a spike region with a radial magnetic field B_R that is sunward. The spike region is separated from the (radially outward) pristine quiet solar wind by transition regions within which B_R reverses (Kasper et al. 2019). The spike region corresponds to a region of enhanced V_R and reversed B_R. Spikes are separated into a core region with plasma conditions that are very different from those of the ambient solar wind, but they are relatively constant. The transition regions on either side of a magnetic spike often contain large-amplitude fluctuations.

A total of 663 magnetic field reversals were identified during the first PSP encounter. Of the 663 identified magnetic field reversals, only 322 (or 49%) events were selected, based on two main criteria that they: (1) contain five magnetically-distinguishable regions, chronologically separated as the leading pristine solar wind (QL), leading transition region (TL; negative-to-positive B_R, in Fig. 1), spike region (SPIKE; steady positive B_R), trailing transition region (TT; positive-to-negative B_R), and trailing solar wind region (QT), and (2) have available quality magnetic and plasma measurements.

2.1. General characteristics

The magnetic and plasma properties in the leading quiet regions and inside switchback spikes were compared across the 322 candidate switchback events. The average duration of the spikes was 190 s.

Figure 2 provides histograms of variations (from the leading quiet, pristine solar wind, "QL", region to the switchback spike region, "SPIKE") in total magnetic field $|B|$, proton density N, proton speed $|V|$, normalized (relative to V_A) proton speed, radial proton temperature derived from the most probable speed W ($\propto T_p^{1/2}$), and plasma beta β_p at leading switchback transition regions. The red dashed lines show the average values.

We note that $|B|$ is slightly reduced across the leading transition regions by $\bar{\mu} = -1.07\%$ ($\sigma = \pm 7.22\%$). The proton density also reduces slightly, $\bar{\mu} = -4.08\%$ ($\pm 10.83\%$). In contrast, the total proton speed (in the spacecraft's frame of reference) is significantly enhanced at the leading switchback transition regions, $\bar{\mu} = +12.63\%$ ($\pm 9.02\%$). It is further shown that the jump in total proton speed is nearly half ($\bar{\mu} = +43.29\%$ ($\pm 27.16\%$)) of the Alfvén velocity in the

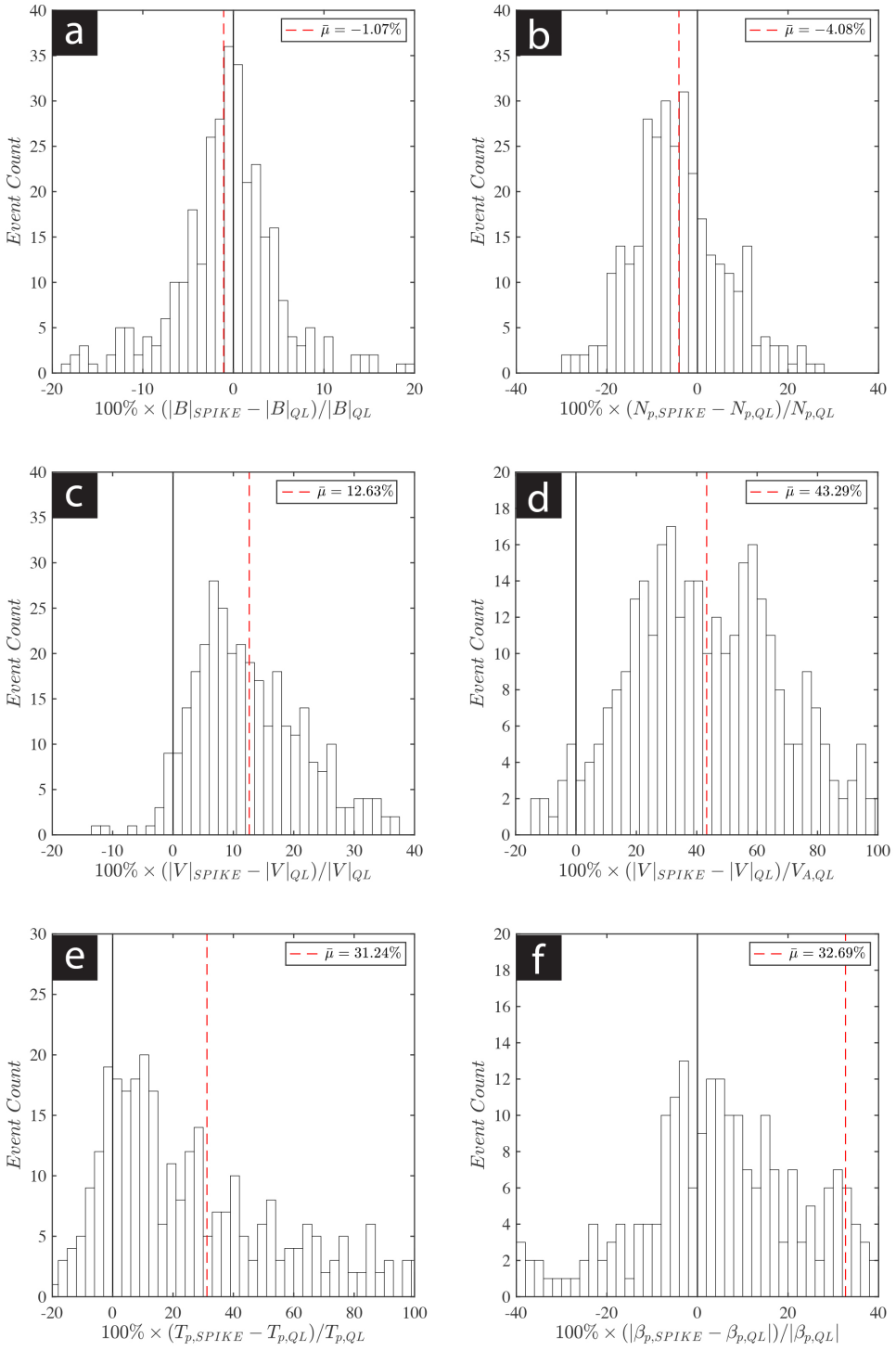

Fig. 2. Histograms of percentage parameter jump across the switchbacks' leading transition regions, $X_{\mathrm{SPIKE}} - X_{\mathrm{QL}}$. Parameters including: (*a*) total magnetic field $|B|$, (*b*) proton density N, (*c*) total proton velocity $|V|$, and (*d*) total proton velocity |V| relative to the local Alfvén velocity V_{A}, (*e*) proton radial temperature T_{p} derived from the most probable speed W, and (*f*) plasma beta β. Parameters are compared at the leading quiet, pristine solar wind (QL) regions and inside the switchback spikes (SPIKE). The red dashed lines indicate the average values $\bar{\mu}$.

upstream pristine solar wind. Radial proton temperature and beta ($\beta = P_{\mathrm{th}}/P_{\mathrm{B}}$) also increase across the switchbacks' leading transition region by $\bar{\mu}$ = +31.24% (±38.86%) and $\bar{\mu}$ = +32.90% (±56.38%), respectively.

Next, magnetic field rotations across the leading and trailing transition regions are determined. The angle $\alpha_{(\mathrm{B\ Q-SPIKE})}$ indicates the change in the magnetic field orientation from the quiet region to the spike: $\alpha_{(\mathrm{B\ Q-SPIKE})} = \arccos((\boldsymbol{B}_{\mathrm{Q}} \cdot \boldsymbol{B}_{\mathrm{SPIKE}})/(|\boldsymbol{B}_{\mathrm{Q}}|\,|\boldsymbol{B}_{\mathrm{SPIKE}}|))$. Figure 3 shows histograms of $\alpha_{(\mathrm{B\ Q-SPIKE})}$ across the leading (blue) and trailing (red) switchback transition regions. On average, it is found that the magnetic field is rotated by $<\alpha_{(\mathrm{B\ Q-SPIKE})}> \sim 60°$ across the leading switchback transition region. The magnetic field returns to its pre-switchback orientation at the trailing boundary.

2.2. Discontinuity analysis

The MVA technique was applied on the 332 switchback transition regions to provide a normal vector $\boldsymbol{n}$ of the directional discontinuity plane (Sonnerup & Cahill Jr 1967). It is important to note that the normal vector, that is to say, the minimum variance direction, was only accurate when the ratio of the intermediate-to-minimum eigenvalues $\lambda_2/\lambda_3 \geq 2.0$ (Lepping & Behannon 1980). This selection criteria disqualifies 59 (or 18%)

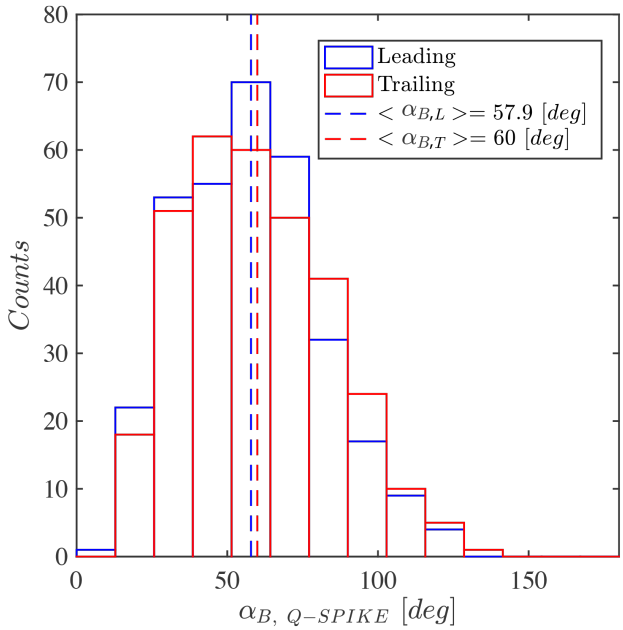

Fig. 3. Histograms of magnetic field rotation $\alpha_{(\mathrm{B\ Q\text{–}SPIKE})}$ across the leading (blue) and trailing (red) switchback transition regions. Average $\alpha_{(\mathrm{B\ Q\text{–}SPIKE})}$ values are shown by dashed lines.

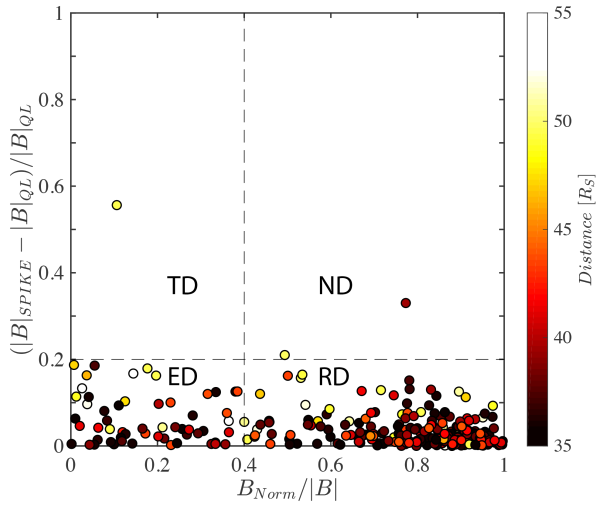

Fig. 4. Discontinuity classification of the 273 magnetic switchbacks. Scatter plot of the relative normal component of magnetic field of upstream, pristine solar wind and the relative variation in magnetic field intensity across the switchbacks' leading (QL-to-SPIKE) transition regions. The color shading indicates the switchbacks' distance from the Sun.

of the 322 switchback events. Nearly half of the remaining 273 qualified switchback events have a $\lambda_2/\lambda_3 \geq 10.0$, indicating exceedingly well-resolved solutions (Behannon et al. 1981). The following discontinuity analyses were applied only on the remaining 273 qualified switchback events.

Neugebauer et al. (1984) classified directional discontinuities in the solar wind observations as rotational (RD), tangential (TD), either (ED), or neither (ND) discontinuity, depending on the relative values of the normal field component $B_{\mathrm{Norm}} \equiv \boldsymbol{B} \cdot \boldsymbol{n}$ and the change in the field magnitude [$|B|$] across the discontinuities. The classification was as follows:

– RD: $|[B_{\mathrm{Norm}}]|/|B| \geq 0.4$ $|[B]|/|B| < 0.2$,
– TD: $|[B_{\mathrm{Norm}}]|/|B| < 0.4$ and $|[B]|/|B| \geq 0.2$,
– ED: $|[B_{\mathrm{Norm}}]|/|B| < 0.4$ and $|[B]|/|B| < 0.2$,
– ND: $|[B_{\mathrm{Norm}}]|/|B| \geq 0.4$ and $|[B]|/|B| \leq 0.2$, and

where $|B|$ in the denominator is the larger of the field magnitudes on either side of the discontinuity.

Figure 4 shows a scatter plot of all 273 qualified discontinuities categorized into four quadrants with respect to their relative magnitudes of $|[B_{\mathrm{Norm}}]| = |B_{\mathrm{Norm,\ SPIKE}} - B_{\mathrm{Norm,\ QL}}|$ and $|[|B|]| = |B_{\mathrm{SPIKE}} - B_{\mathrm{QL}}|$ across their leading (QL-to-SPIKE) transition regions. The resulting populations of discontinuities in each category are RD:TD:ED:ND = 214:1:56:2. The shading of the markers indicates the discontinuity's distance from the Sun.

It is found that the relative change in $|[|B|]|$ increases with distance from the Sun. Of the 214 leading RD-type switchback transition regions, 122 have $0.8 < |[B_{\mathrm{Norm}}]|/|B| < 1.0$ and are observed closest to the Sun at $r < 40$ Sun radii ([R_S]).

Figure 5a shows scatter plot of RD-to-ED event count ratios as a function of the distance from the Sun. The number of events in each radial bin (bin width = 1 [R_S]) is presented in blue. It is found that the relative number of RD-type leading transition regions reduces at an average rate of -0.14 [R_S^{-1}] with an increasing distance from the Sun. The linear fit's y-intercept suggests that the RD-to-ED ratio is ∼10 in the solar atmosphere.

3. Discussion

In this study, MVA was applied to 322 quality switchback transition regions to determine discontinuity normals, and 49 switchback normals were disqualified because $(\lambda_2/\lambda_3) < 2$. These surface normals may have been impacted by surface waves on the discontinuities (Horbury et al. 2001).

The remaining 273 qualified leading switchback transition regions indicate that:

First, the magnetic switchbacks' leading transition regions are mostly (78%) RD-type discontinuities, consistent with Larosa et al. (2021). ED accounts for another 21% of the leading switchback transition regions. It is also found that the ratio of RD-to-ED counts decreases with an increasing distance from the Sun, suggesting that either (a) leading switchback transition regions evolve from RD-type into ED-type discontinuities as they propagate away from the Sun, or (b) local switchback generation mechanisms change with distance from the Sun (Zank et al. 2020).

Figure 5b juxtaposes the RD-to-ED ratio near the Sun with those of Yamauchi et al. (2002) where 100 non-PBS events with B_{R} reversals were investigated in Ulysses observations off the ecliptic plane at 1.63–3.73 AU. As shown farther from the Sun, the RD-to-ED ratio has changed from 4:1 at 0.2 AU to 1:3 at 2.5 AU. These results further suggest that leading switchback transition regions evolve from RD- into ED-type discontinuities as they propagate away from the Sun. Furthermore, the discontinuities at 1 AU have been reported as RD:ED ∼ 2 : 1 (e.g., Neugebauer et al. 1984; Horbury et al. 2001; Lepping & Behannon 1980). However, these studies have a different discontinuity selection criteria, in particular the B_{R} reversal requirement.

Second, total pressure remains relatively constant across the RD-type switchback transition regions $(P_{\mathrm{tot,SPIKE}} - P_{\mathrm{tot,QL}})/P_{\mathrm{tot,QL}} = +0.04$, which is in agreement with PBSs in Ulysses observations (Yamauchi et al. 2002).

The magnetic field magnitude reduces only slightly (−1%) across the leading switchback transition regions (Farrell et al. 2020; Agapitov et al. 2020). Strong $|B|$ potentially helps switchbacks remain stable while propagating (Landi et al. 2006;

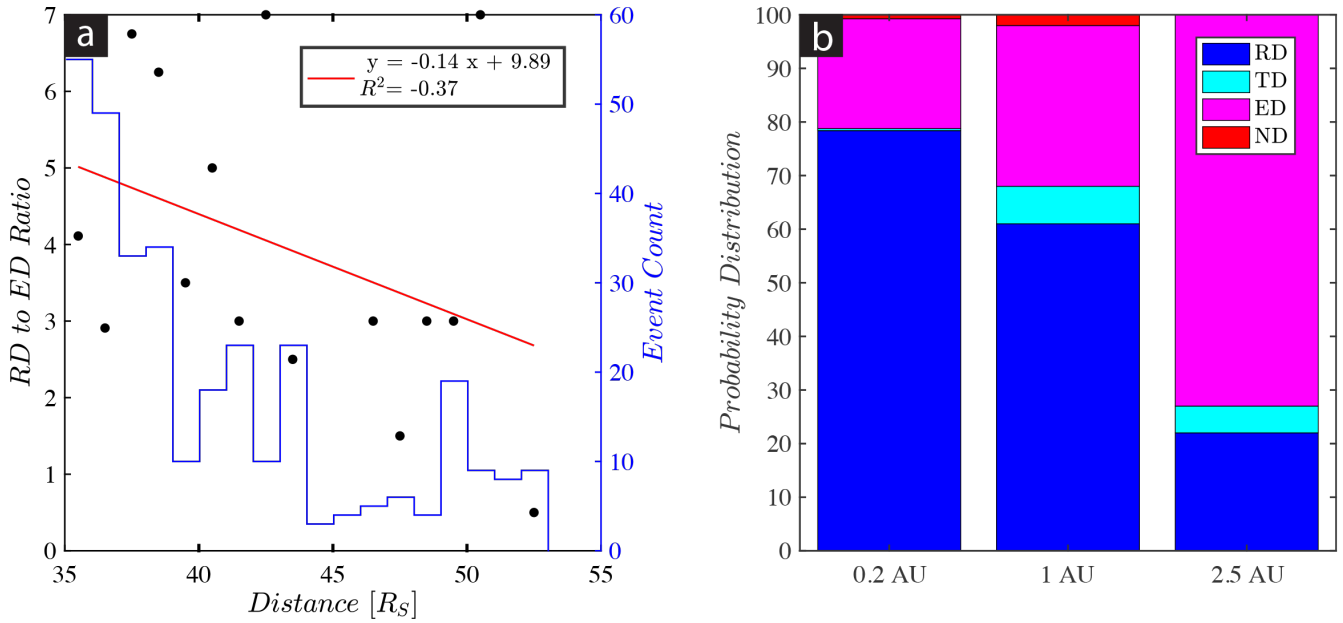

Fig. 5. (*a*) Scatter plot of the ratio of number of RD events to that of ED as a function of distance from the Sun. The histogram of event count per radial distance (bin width = 1 [R_S]) is provided on the right y-axis in blue for reference. (*b*) Stacked bar plots of the relative ratios of RD:TD:ED:ND discontinuities for the present study (PSP@0.2 AU) and the studies by Neugebauer et al. (1984, ISEE@1.0 AU) and Yamauchi et al. (2002, Ulysses@1.63–3.73 AU).

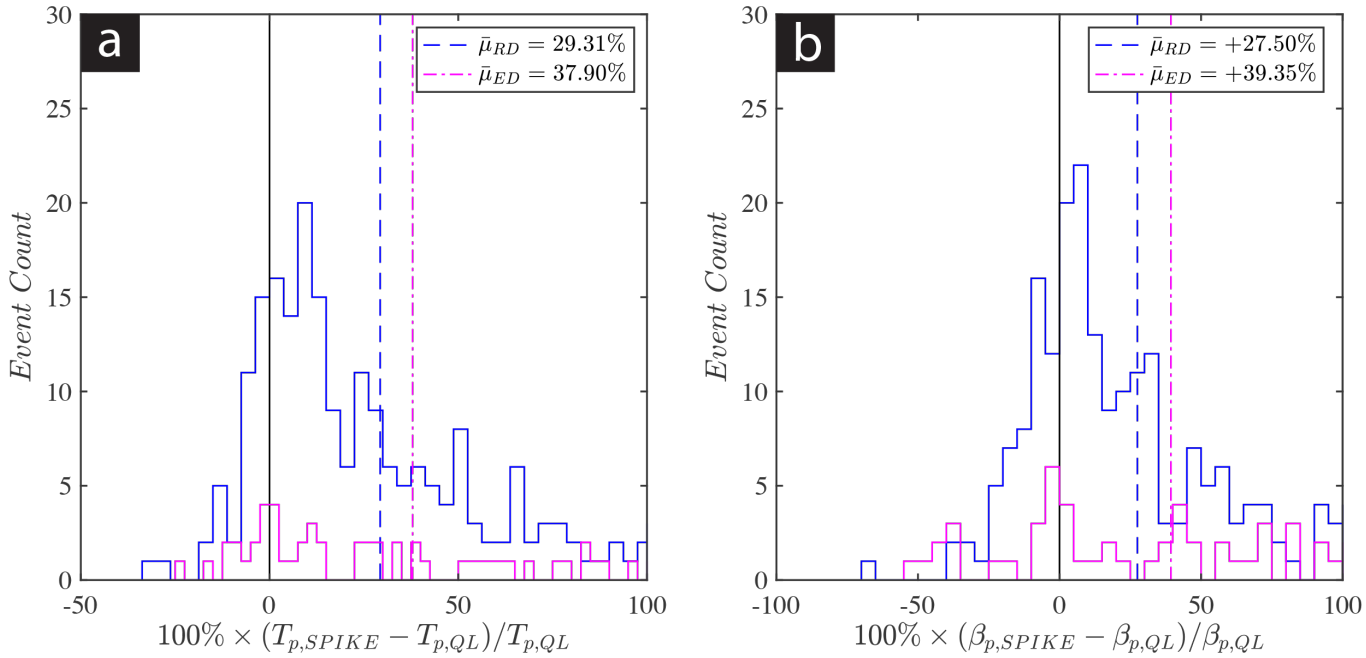

Fig. 6. Histograms of the relative (*a*) proton temperature, and (*b*) plasma beta jumps across the RD- (blue) and ED-type (magenta) switchback transition regions, ($\beta_{\rm SPIKE} - \beta_{\rm QL}$)/$\beta_{\rm QL}$. Average values are shown by dashed lines.

Tenerani et al. 2020). Similarly, magnetic pressure is only reduced by ∼−1.4% at leading RD-type switchback transition regions.

Thermal pressure jumps by +26.70% at the leading transition regions. Plasma density is found to reduce slightly (by −4.08%) across the leading transition regions. On the other hand, the proton temperature changes significantly (+31.24%) at the leading switchback transition regions.

Figure 6a shows the jumps in the radial proton temperature in the leading RD- and ED-type switchback transition regions. The jump in proton temperature is found to be more significant across the leading ED-type (+37.9%) switchback transition regions than the RD-type switchback transition regions ($\Delta T_{\rm p}/T_{\rm p}$ = +37.9%, corresponding to $\Delta P_{\rm th}/P_{\rm th}$ = +24.2%). Plasma acceleration and heating processes in low-beta environments remain open science questions (Akhavan-Tafti et al. 2019b, 2020a,b; Drake et al. 2019).

Figure 6b shows the jumps in plasma beta $\beta_{\rm p}$ in the leading RD- and ED-type switchback transition regions. It is found that $\beta_{\rm p}$, on average, increases by +27.5% at the leading RD-type

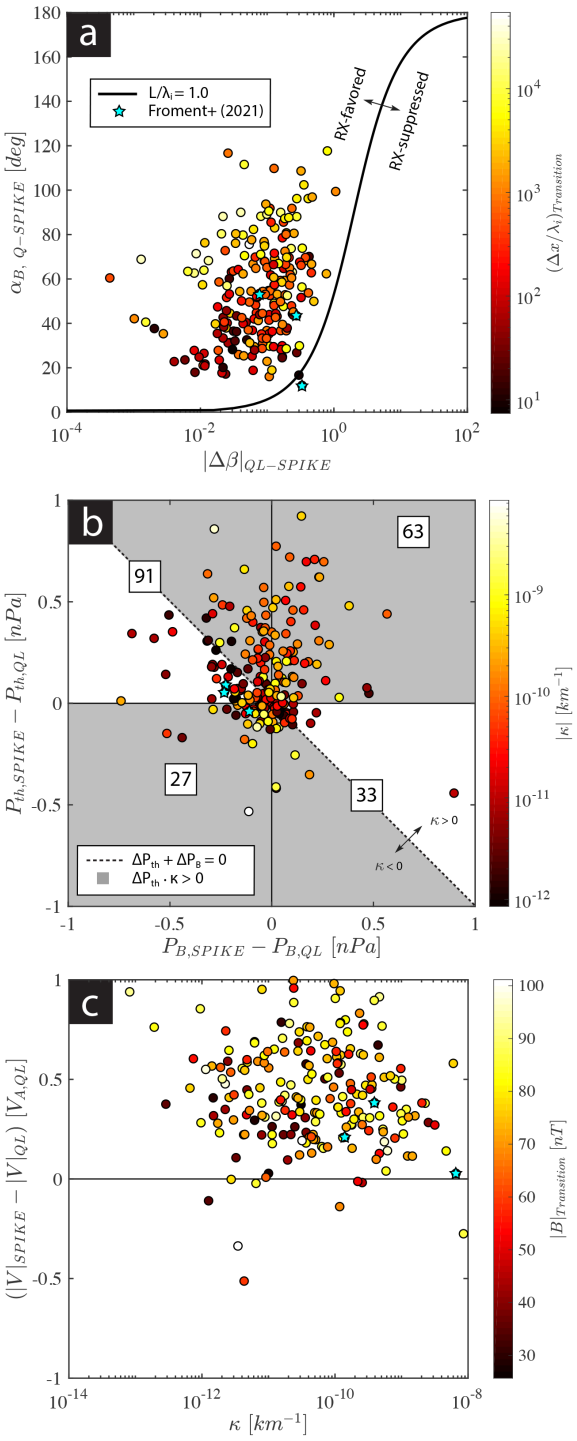

Fig. 7. Scatter plots of parameters at the 214 leading RD-type switchback transition regions: (*a*) Plasma beta variations and magnetic shear angles. The solid curve shows $|\Delta\beta| = 2(L/\lambda_i)\ \tan(\alpha/2)$ for $(L/\lambda_i) = 1.0$. The shading indicates the switchback transition region's normalized thickness $\Delta x/\lambda_i$. The cyan stars correspond to the reconnecting leading switchback transition regions reported by Froment et al. (2021). (*b*) Variations in thermal and magnetic pressures. The values in each box determine the number of the RD-type transition regions in each quadrant. The color shading indicates $|\kappa| = |(\boldsymbol{b}\cdot\nabla)\boldsymbol{b}| = \mu_0\,|\Delta P_{\rm th} + \Delta P_{\rm B}|/B^2_{\rm QL}$. The gray shaded regions show where $\kappa \cdot \Delta P_{\rm th} > 0$ (bad curvature). The dashed line represents the curve along which $\Delta P_{\rm th} + \Delta P_{\rm B} = 0$ (referred to as the total-pressure balance). (*c*) κ and the normalized proton speed variations. The shading indicates the average magnetic field magnitude inside the leading transition regions, $|B|_{\rm Transition}$.

switchback transition regions. The jump in $\beta_{\rm p}$ is more significant (+39.35%) at the leading ED-type switchback transition regions.

Figure 6b shows that both the leading RD- and ED-type switchback transition regions have jumps in $\beta_{\rm p}$ (RD : ED = +27.5% : +39.35%). Therefore, the evidence suggests the following: (1) local proton heating mechanisms may be present within the leading transition regions (Akhavan-Tafti et al. 2019a), (2) the quiet and spike regions originate from different sources (Zank et al. 2020), and/or (3) the quiet and spike regions are driven by different evolution mechanisms (Macneil et al. 2020; Drake et al. 2021). Future investigations shall study the evolution of adiabatic invariants across the switchback transition regions to shed light on potential plasma acceleration and/or heating in the leading switchback transition regions. Nonadiabatic plasma heating mechanisms (electromagnetic waves; Krasnoselskikh et al. 2020) at the boundaries of the switchbacks (especially in 'complex switchback structures,' defined as the aggregation or clustering of switchbacks de Wit et al. 2020) are also of significant importance (Zank et al. 2020; Mozer et al. 2020).

Third, no net magnetic shear is caused in pristine solar wind by the switchbacks, suggesting that pre- and post-switchback solar wind magnetic fields may have originated from the same source region (Larosa et al. 2021). The magnetic field reverses at the leading switchback transition region by first rotating at $<\alpha_{(\rm B\ QL-SPIKE)}> \sim 60°$. The magnetic field vector flips back to its pre-switchback orientation at the trailing boundary, $<\alpha_{(\rm B\ QT-SPIKE)}> \sim 60°$.

Fourth, the angle between the leading pristine solar wind and the switchback spike $\alpha_{(\rm BQ-SPIKE)} \sim 60°$ can also be thought of as magnetic shear angle. Krasnoselskikh et al. (2020) show that the shear angle across switchback transition regions creates current surfaces that isolate magnetic spikes, likely twisted magnetic flux tubes (analogous to flux ropes; Akhavan-Tafti et al. 2018), from pristine solar wind. The magnetic shear angle is a determining factor in magnetic reconnection (Swisdak et al. 2003).

The evidence presented in this study that magnetic switchback transition regions may evolve (from RD-type into ED-type) as they propagate away from the Sun raises two new science questions: (1) does magnetic reconnection take place in the switchback transition regions? Surprisingly, Phan et al. (2020) have reported that no reconnection signatures were observed inside the switchback transition regions, suggesting that switchbacks are isolated RD-type current sheets that do not undergo reconnection. On the other hand, Froment et al. (2021) have recently provided direct evidence for magnetic reconnection occurring within the switchback transition regions, and (2) if magnetic reconnection does not commonly occur, what is the source (generation and/or evolution mechanisms) of the observed proton temperature increase (Woodham et al. 2021) at the leading switchback transition regions? Recently, Woolley et al. (2020) have shown that the parallel proton temperature does not vary across the switchback transition regions, further highlighting the role of local mechanisms in switchback evolution.

Here, we focus on the former science question by investigating whether the leading RD-type switchback transition regions do in fact provide the appropriate environment for magnetic reconnection to occur.

Figure 7a shows a scatter plot of the distribution of plasma beta variations and magnetic shear angles across the 214 leading RD-type switchback transition regions. The shading indicates the normalized thickness ($\Delta x/\lambda_i$; where Δx and λ_i are switchback transition region thickness and local ion (in this case,

proton) inertial length, respectively) of switchback transition regions. It is found that all but one of the RD-type switchbacks' leading transition regions theoretically favor magnetic reconnection for $L/\lambda_i = 1.0$ (solid curve; Swisdak et al. 2003), where L denotes current sheet thickness. The switchback transition region thickness Δx was determined using the normal velocity component to avoid spacecraft trajectory bias (Laker et al. 2021). As the shading indicates, all of the RD-type switchback transition regions have a thickness that is larger (or significantly larger) than the local ion inertial length, therefore favoring reconnection. According to Froment et al. (2021), the reconnecting switchback transition regions, as marked by cyan stars, had thicknesses ranging between 10 and $200\lambda_i$.

Figure 7b shows a scatter plot of the variations of thermal and magnetic pressures across the 214 leading RD-type transition regions. The color shading indicates the magnetic curvature magnitude, defined as $|\kappa| = |(\boldsymbol{b}\cdot\nabla)\boldsymbol{b}|$. To estimate κ, it was assumed that the leading RD-type transition regions are "stable" (Landi et al. 2005), hence, at force-balance, $\boldsymbol{j}\times\boldsymbol{B} - \nabla\boldsymbol{P}_{\rm th} = 0$, where $\boldsymbol{j}$ is the current density. The assumption allowed us to estimate the magnetic field curvature as $\kappa = (\boldsymbol{b}\cdot\nabla)\boldsymbol{b} = \mu_0\,(\nabla P_{\rm th} + \nabla P_{\rm B})/|B|^2 \sim (\mu_0/\Delta x)\,(\Delta P_{\rm th} + \Delta P_{\rm B})/|B|^2$ (Akhavan-Tafti et al. 2019a).

The total pressure remains relatively constant ($\bar{\mu}_{\Delta P,\rm tot} \sim +4\%$) at the leading RD-type transition regions, ($P_{\rm tot,SPIKE} \sim P_{\rm tot,QL}$). This means that the jump in the thermal pressure gradient $\Delta P_{\rm th}$ is often balanced by a magnetic pressure gradient $\Delta P_{\rm B}$, therefore resulting in a negligible magnetic curvature, that is to say the magnetic tension force. But, on average, the magnetic pressure gradient remains relatively constant ($\bar{\mu}_{\Delta P,B} \sim -1.4\%$) at the leading RD-type transition regions, suggesting that a magnetic tension force must increase to balance $\Delta P_{\rm th}$.

Of the 214 leading RD-type transition regions, only 56 are characterized as having a "good" curvature (that is antiparallel magnetic curvature and thermal pressure gradient: $\kappa\cdot\nabla P_{\rm th} < 0$). The remaining 158 leading RD-type transition regions (74%) have "bad" curvatures, hence unstable. The reconnecting leading switchback transition regions of Froment et al. (2021) all lie below the dashed line in the region where $\kappa < 0$, suggesting that magnetic reconnection may only occur within leading switchback transition regions where the total pressure of the switchback spike is smaller than that in pristine solar wind, $\Delta P_{\rm tot} = P_{\rm tot,SPIKE} - P_{\rm tot,QL} < 0$. Furthermore, the reconnecting current sheets are observed in both theoretically stable and unstable (prone to plasma "ballooning" instability) plasma environments, as indicated by the cyan stars in the white- and gray-shaded regions of the plot, respectively.

Magnetic curvature plays a key role in magnetic reconnection (Petschek 1964) as well as particle heating and acceleration (Drake et al. 2006; Akhavan-Tafti et al. 2019b). On average, the curvature of the reconnecting switchback current sheets is $\bar{\mu}_\kappa = -2.38\,(\pm 3.65)\times 10^{-9}$ [km^{-1}]. This value is by several orders of magnitude smaller than curvatures often observed at or near reconnecting current sheets at 1 AU (Akhavan-Tafti et al. 2019a; Bandyopadhyay et al. 2020; Yang et al. 2019; Norgren et al. 2018). This may be an artifact of how κ is determined here (using single-spacecraft measurements).

Figure 7c shows a scatter plot of κ and velocity variations (relative to local $V_{\rm A}$) across the 214 leading RD-type transition regions. The color shading shows the average magnetic field intensity inside the switchbacks' leading transition regions, $|B|_{\rm Transition}$. The figure indicates that (1) there is no clear (anti)correlation between magnetic curvature and $|B|_{\rm Transition}$ (Bandyopadhyay et al. 2020) in leading RD-type switchback transition regions ($\bar{\mu}_{|B|,\rm Transition} = 43.2\ (\pm 16.9)\ [nT]$), and (2) the reconnecting leading switchback transition regions of Froment et al. (2021) are characterized by small and positive relative jump in proton velocity $0 < |V|_{\rm SPIKE} - |V|_{\rm QL} < 0.5\ V_{\rm A,QL}$. Particle-in-Cell (PIC) simulations by Swisdak et al. (2003) suggest that diamagnetic drifts can suppress reconnection when the velocity of the convecting structure becomes comparable to the local Alfvén velocity.

To summarize, we find that the leading RD-type switchback transition regions provide reconnection-favorable plasma and magnetic conditions, including plasma beta ($|\Delta\beta|$), shear angle ($\alpha_{\rm B}$), relative current sheet thickness ($\Delta x/\lambda_i$), and relative velocity shear ($|\Delta V|/V_{\rm A}$). However, inside the leading switchback transition regions (1) magnetic curvature (κ) is often negligible (that is to say negligible magnetic twist or tension force), and (2) the magnetic field strength ($|B|_{\rm Transition}$) is too large, therefore potentially suppressing magnetic reconnection by preventing instability formation and growth (Landi et al. 2005), such as current sheet thinning in the case of tearing-mode instability (Parker 1957, 1958; Furth et al. 1963).

4. Conclusion

In conclusion, 78% of the leading switchback transition regions are RD-type discontinuities. The leading switchback transition regions may evolve from RD-type into ED-type discontinuities while propagating away from the Sun. Local magnetic reconnection is likely not the main driver of this evolution. Other drivers, such as local plasma acceleration and/or heating mechanisms need to be investigated to explain the observed significant jump (+29.31%) in the proton temperature and the prevalence (74%) of bad curvature at the leading RD-type switchback transition regions.

Acknowledgements. The authors would like to thank the Solar Parker Probe team that enabled this study. The research done at the University of Michigan was supported by NNN06AA01C and 80NSSC20K1847. The research done at École Polytechnique was supported by the DGA project, École Polytechnique, Université Paris–Saclay, convention 2778/IMES.

References

Agapitov, O. V., de Wit, T. D., Mozer, F. S., et al. 2020, ApJ, 891, L20
Akhavan-Tafti, M., Slavin, J. A., Le, G., et al. 2018, J. Geophys. Res.: Space Phys, 123, 1224
Akhavan-Tafti, M., Slavin, J., Eastwood, J., Cassak, P., & Gershman, D. 2019a, J. Geophys. Res.: Space Phys, 124, 5376
Akhavan-Tafti, M., Slavin, J. A., Sun, W. J., Le, G., & Gershman, D. J. 2019b, Geophys. Res. Lett., 46, 12654
Akhavan-Tafti, M., Palmroth, M., Slavin, J. A., et al. 2020a, J. Geophys. Res.: Space Phys, 125, e2019JA027410
Akhavan-Tafti, M., Fontaine, D., Slavin, J. A., Le Contel, O., & Turner, D. 2020b, J. Geophys. Res.: Space Phys., 125, e2020JA028027
Bale, S. D., Goetz, K., Harvey, P. R., et al. 2016, Space Sci. Rev., 204, 49
Bale, S. D., Badman, S. T., Bonnell, J. W., et al. 2019, Nature, 576, 237
Bandyopadhyay, R., Yang, Y., Matthaeus, W. H., et al. 2020, ApJ, 893, L25
Behannon, K. W., Neubauer, F. M., & Barnstorf, H. 1981, J. Geophys. Res.: Space Phys., 86, 3273
Borovsky, J. E. 2016, J. Geophys. Res.: Space Phys., 121, 5055
de Wit, T. D., Krasnoselskikh, V. V., Bale, S. D., et al. 2020, ApJS, 246, 39
Drake, J. F., Swisdak, M., Che, H., & Shay, M. A. 2006, Nature, 443, 553
Drake, J. F., Arnold, H., Swisdak, M., & Dahlin, J. T. 2019, Phys. Plasmas, 26, 12901
Drake, J. F., Agapitov, O., Swisdak, M., et al. 2021, A&A, 650, A2 (PSP SI)
Farrell, W. M., MacDowall, R. J., Gruesbeck, J. R., Bale, S. D., & Kasper, J. C. 2020, ApJS, 249, 28
Fox, N. J., Velli, M. C., Bale, S. D., et al. 2016, Space Sci. Rev., 204, 7
Froment, C., Krasnoselskikh, V., Dudok de Wit, T. D., et al. 2021, A&A, 650, A5 (PSP SI)

Furth, H. P., Killeen, J., & Rosenbluth, M. N. 1963, Phys. Fluids, 6, 459
Horbury, T. S., Burgess, D., Fränz, M., & Owen, C. J. 2001, Geophys. Res. Lett., 28, 677
Horbury, T. S., Woolley, T., Laker, R., et al. 2020, ApJS, 246, 45
Kahler, S. W., Crocker, N. U., & Gosling, J. T. 1996, J. Geophys. Res.: Space Phys., 101, 24373
Kasper, J. C., Abiad, R., Austin, G., et al. 2016, Space Sci. Rev., 204, 131
Kasper, J. C., Bale, S. D., Belcher, J. W., et al. 2019, Nature, 576, 228
Krasnoselskikh, V., Larosa, A., Agapitov, O., et al. 2020, ApJ, 893, 93
Laker, R., Horbury, T. S., Bale, S. D., et al. 2021, A&A, 650, A1 (PSP SI)
Landi, S., Hellinger, P., & Velli, M. 2005, in Solar Wind 11/SOHO 16, Connecting Sun and Heliosphere, 592, 785
Landi, S., Hellinger, P., & Velli, M. 2006, Geophys. Res. Lett., 33, L14101
Larosa, A., Krasnoselskikh, V., Dudok de Wit, T., et al. 2021, A&A, 650, A3 (PSP SI)
Lepping, R. P., & Behannon, K. W. 1980, J. Geophys. Res.: Space Phys., 85, 4695
Macneil, A. R., Owens, M. J., Wicks, R. T., et al. 2020, MNRAS, 494, 3642
Matteini, L., Horbury, T. S., Neugebauer, M., & Goldstein, B. E. 2014, Geophys. Res. Lett., 41, 259
McComas, D. J., Hoogeveen, G. W., Gosling, J. T., et al. 1996, A&A, 316, 368
Mozer, F. S., Agapitov, O. V., Bale, S. D., et al. 2020, ApJS, 246, 68
Neugebauer, M., Clay, D. R., Goldstein, B. E., Tsurutani, B. T., & Zwickl, R. D. 1984, J. Geophys. Res.: Space Phys., 89, 5395
Norgren, C., Graham, D. B., Khotyaintsev, Y. V., et al. 2018, J. Geophys. Res.: Space Phys., 123, 9222
Parker, E. N. 1957, J. Geophys. Res., 62, 509
Parker, E. N. 1958, Phys. Fluids, 1, 171
Petschek, H. E. 1964, NASA Spec. Publ., 50, 425
Phan, T. D., Bale, S. D., Eastwood, J. P., et al. 2020, ApJS, 246, 34
Sonnerup, B. U. O., & Cahill Jr, L. J. 1967, J. Geophys. Res., 72, 171
Squire, J., Chandran, B. D. G., & Meyrand, R. 2020, ApJ, 891, L2
Suess, S. T. 2007, in Second Solar Orbiter Workshop, 641
Swisdak, M., Rogers, B. N., Drake, J. F., & Shay, M. A. 2003, J. Geophys. Res.: Space Phys., 108, 1218
Tenerani, A., Velli, M., Matteini, L., et al. 2020, ApJS, 246, 32
Tsurutani, B. T., & Smith, E. J. 1979, J. Geophys. Res.: Space Phys., 84, 2773
Tsurutani, B. T., Lakhina, G. S., Verkhoglyadova, O. P., et al. 2011, J. Atm. Solar-Terrestrial Phys., 73, 5
Woodham, L. D., Horbury, T. S., Matteini, L., et al. 2021,A&A, 650, L1 (PSP SI)
Woolley, T., Matteini, L., Horbury, T. S., et al. 2020, MNRAS, 498, 5524
Yamauchi, Y., Suess, S. T., & Sakurai, T. 2002, Geophys. Res. Lett., 29, 21
Yamauchi, Y., Suess, S. T., Steinberg, J. T., & Sakurai, T. 2004, J. Geophys. Res.: Space Phys., 109, 1
Yang, Y., Wan, M., Matthaeus, W. H., et al. 2019, Phys. Plasmas, 26, 72306
Zank, G. P., Nakanotani, M., Zhao, L.-L., Adhikari, L., & Kasper, J. 2020, ApJ, 903, 1